

† . \* . \* . \* . \*\*

## Application of Laser Interferometry for Assessment of Surface Residual Stress by Determination of Stress-free State

Dong-Won Kim, Nak-Kyu Lee, Tae-Hoon Choi, Kyoung-Hoan Na and Dongil Kwon

**Key Words :** Nondestructive Test(가), Interferometry( ), Annealing( ), Thermo-elastic( ), Residual Stress( ), Mapping( ).

### Abstract

The total relaxed stress in annealing and the thermal strain/stress were obtained from the identification of the residual stress-free state using electronic speckle pattern interferometry (ESPI). The residual stress fields in case of both single and film/substrate systems were modeled using the thermo-elastic theory and the relationship between relaxed stresses and displacements. We mapped the surface residual stress fields on the indented bulk Cu and the 0.5 μm Au film by ESPI. In indented Cu, the normal and shear residual stress are distributed over -1.7 GPa to 700 MPa and -800 GPa to 600 MPa respectively around the indented point and in deposited Au film on Si wafer, the tensile residual stress is uniformly distributed on the Au film from 500 MPa to 800 MPa. Also we measured the residual stress by the x-ray diffractometer (XRD) for the verification of above residual stress results by ESPI.

$\Delta\Phi$ :  
 $\lambda$ :  
 $d$ :  
 $\alpha$ :  
 $\beta$ :  
 $f$ :  
 $\sigma_{ii}^r$ :  
 $\epsilon_{ii}^m$ :  
 $\epsilon_{ii}^f$ :

$\Delta\alpha$ :  
 $\Delta T_d$ :  
 $\epsilon_{ii}^{r*}$ :  
 $\epsilon^a$ :  
 $\Delta T_a$ :  
 $\theta$ :  
 $\Psi$ : x-ray source

(= )  
 (1-D )  
 (1-D )  
 x-ray source

†

E-mail : dongwonk@gong.snu.ac.kr  
 TEL : (02)880-8025 FAX : (02)889-4380

\*

\*\*

1.

drilling method

hole-

가 (1,2),  
 X-ray,  
 Barkhausen noise  
 가 가 (3-5)  
 (mapping)

, FEA(Finite Element Analysis)  
 가 가  
 (6) 가 가  
 in- situ  
 ESPI (Electronic Speckle  
 Pattern Interferometry)  
 Au Cu 가

2. ESPI

ESPI 가  
 (speckle)  
 (beam splitter)  
 (reference beam) (object beam)  
 CCD 가  
 가

Fig. 1(a)

$$\Delta\Phi = \left(\frac{2\pi}{\lambda}\right) \times [d(\sin\alpha + \sin\beta)] \quad (1)$$

(2) 가  
 가  

$$d = \frac{f\lambda}{\sin\alpha + \sin\beta} \quad (2)$$
  
 Fig. 1(b) 가

(3) 가  
 (7)  

$$d = \frac{f\lambda}{2\sin\alpha} \quad (3)$$
  
 (2), (3)  
 (phase shift method)

256  
 phase  
 4  
 (4) 가 (8)  
 가  
 (working  
 distance)  
 (x2)  
 1~20 가

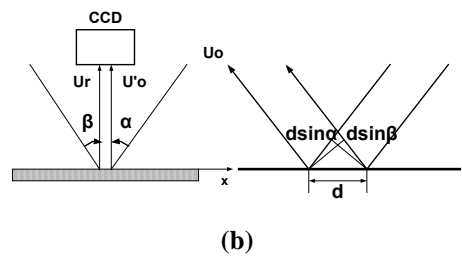
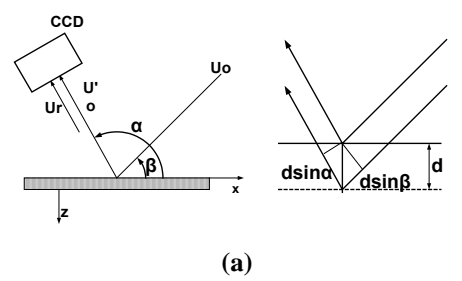


Fig. 1 Schematic diagram of evolving (a) out-of-plane and (b) in-plane displacements.

3. ESPI

3.1 ESPI

(element)

3.3

가

(compatibility)

가

가

(9)

6

(6)

$$\begin{aligned} \varepsilon_{xx}^r &= \frac{1}{E} (\sigma_{xx}^r - \nu \sigma_{yy}^r) = -\Delta\alpha\Delta T_d + \varepsilon_{xx}^{r*} \\ \varepsilon_{yy}^r &= \frac{1}{E} (\sigma_{yy}^r - \nu \sigma_{xx}^r) = -\Delta\alpha\Delta T_d + \varepsilon_{yy}^{r*} \end{aligned} \quad (6)$$

가

가

가

가

가

가

가

(10). ESPI in-situ

가

ESPI

3.2

가

( (7), Fig. 2).

(9)

가

$$\begin{aligned} \varepsilon^m &= -\varepsilon^r - \varepsilon^a \\ &= \Delta\alpha\Delta T_d - \varepsilon^{r*} + \Delta\alpha\Delta T_a \end{aligned} \quad (7)$$

(6) (7)

(8)

가 ( (4)).

$$\sigma^r = -\sigma^{rel} \quad (4)$$

ESPI

가

$$\sigma_{xx}^r = -\frac{E}{1-\nu^2} (\varepsilon_{xx}^m + \nu\varepsilon_{yy}^m) + \frac{E}{1-\nu} \Delta\alpha\Delta T_a \quad (8)$$

$$\sigma_{yy}^r = -\frac{E}{1-\nu^2} (\varepsilon_{yy}^m + \nu\varepsilon_{xx}^m) + \frac{E}{1-\nu} \Delta\alpha\Delta T_a$$

(8)

(4) ( (5)).

가

$$\begin{aligned} \sigma_{xx}^r &= -\frac{E}{1-\nu^2} (\varepsilon_{xx}^m + \nu\varepsilon_{yy}^m) \\ \sigma_{yy}^r &= -\frac{E}{1-\nu^2} (\varepsilon_{yy}^m + \nu\varepsilon_{xx}^m) \\ \tau_{xy}^r &= -G\gamma_{xy}^m \end{aligned} \quad (5)$$

( )

가

(8)

가

(5)

가

(8)

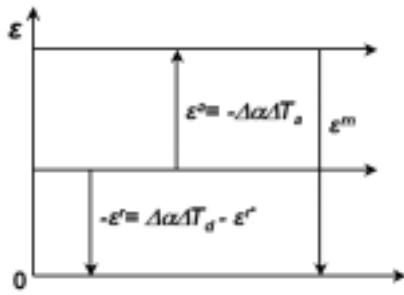


**Fig. 2** Schematic diagram of the relationship among the variations of the residual strain, the thermal strain in interface and the strain evaluated by ESPI.

4.

4.1

(annealing)

ESPI

(  $10^{-3}$ Torr)

가

(quartz)

214 mm

$\pm 1$

4.2

400  $\mu$ m

3 $\times$ 3 mm<sup>2</sup>

110GPa

Cu

0.35

, ESPI

185 min

20

300~

420

3(a)

(A,B,C,D)

(Fig. 3(b)). Fig.

3(b)

400

400~420

185min

가

(5)

Fig. 4

Fig. 4 (a)

(b) (c)

yz xz

Fig. 4(b) (c)

yz xz

가

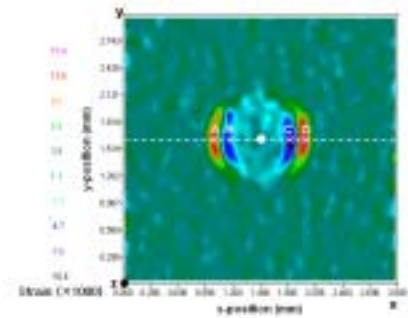
-1.7GPa~700MPa

-800~600MPa

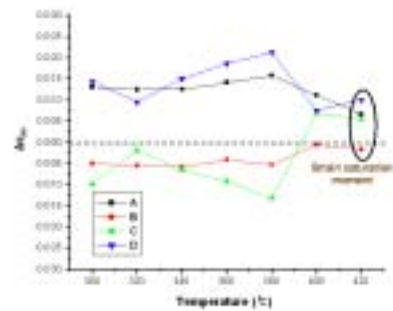
가

pile-up

가

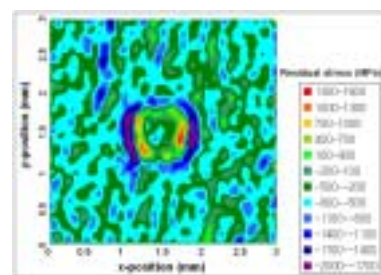


(a)

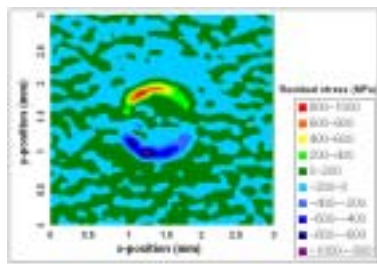


(b)

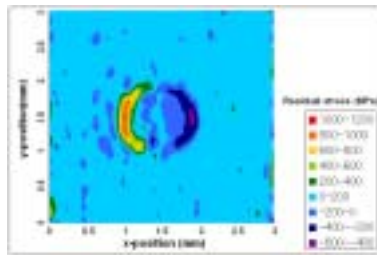
**Fig. 3** (a) 4 arbitrary points (A, B, C and D indicating max. and min. normal strains) on the map of x-dir. normal strains at 300 and (b) the variations in the strain changes in annealing at the 4 arbitrary points in indented Cu.



(a)



(b)



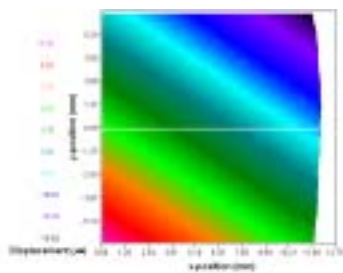
(c)

**Fig. 4** The maps of (a) normal residual stress field in x direction and surface shear residual stress fields in (b) y-z and (c) x-z directions of indented Cu.

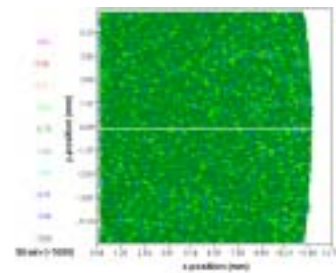
4.2 Au 가  
 500  $\mu\text{m}$  Si 0.1  $\mu\text{m}$  Cr  
 0.5  $\mu\text{m}$  Au 가 170min  
 ~400 50 250  
 12.75mm<sup>2</sup> , Au Si 12.75  $\times$   
 107GPa Au 0.44 Au 74  
 Si 13.8  $\times 10^{-6}$  / 2.6  
 $\times 10^{-6}$  /  
 400 170min x

Fig. 5

, y=0 Fig. 6(a)  
 (b) 400 , 170  
 min 가

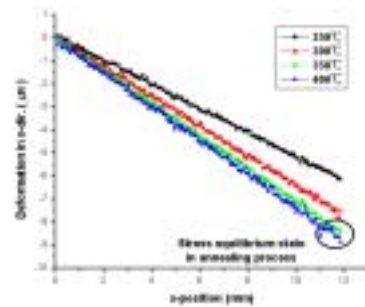


(a)

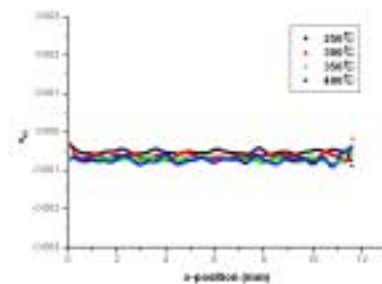


(b)

**Fig. 5** (a) The displacement and (b) the normal strain maps in x-direction at 400°C annealing.



(a)

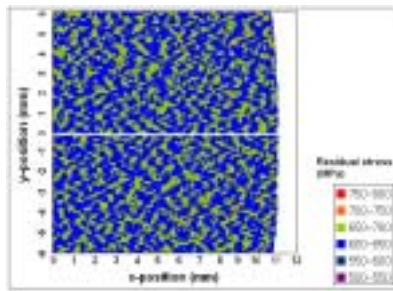


(b)

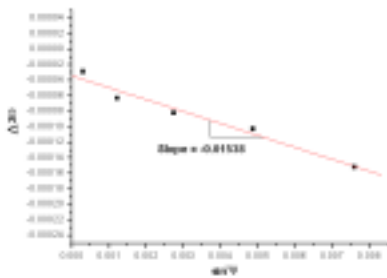
**Fig. 6** The variations of (a) the deformation and (b) the normal strain profiles in x-direction on y=0 line at each annealing temperature.

(8) x  
 (Fig. 7(a)).

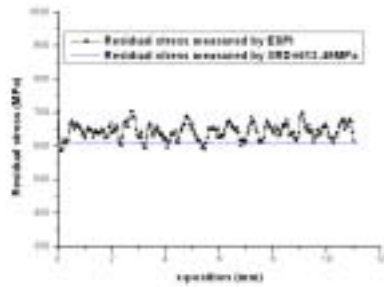
Au  
 500~800MPa 가  
 x-ray  
 diffractometer(XRD) 가  
 (Fig. 7(b)), 612.49MPa  
 가 ESPI  
 (Fig. 7(c)).



(a)



(b)



(c)

**Fig. 7** (a) The normal residual stress field in x-direction, (b) the relationship of variation of  $2\theta$  and  $\sin^2\psi$  in XRD test and (c) the residual stress profile on  $y=0$  line of  $0.5 \mu\text{m}$  Au film .

5.

ESPI

가  
Cu Au  
가

pile-up

Au

ESPI  
XRD

- (1) D. V. Nelson and A. Makino, The holographic- hole drilling method for residual stress determination, *Optics and Laser in Engineering*, Vol. 27, 1997, pp. 3-23.
- (2) Ignacio H. Lira, Cristiān Vial and Kimberly Robinson, The ESPI measurement of the residual stress distribution in chemically etched cold-rolled metallic sheets, *Measurement of Science Technology*, Vol. 8, 1997, pp. 1250-1257.
- (3) Bernd Kämpfe, Investigation of residual stresses in microsystems using X-ray diffraction, *Materials Science and Engineering A*, Vol. 288, No. 2, 2000, pp. 119-125.
- (4) G. A. Webster and R. C. Wimpory, Non- destructive measurement of residual stress by neutron diffraction, *Journal of Materials Processing Technology*, Vol. 117, No. 3, 2001, pp. 395-399.
- (5) J. Gauthier, T. W. Krause and D. L. Atherton, Measurement of residual stress in steel using the magnetic Barkhausen noise technique, *NDT & E International*, Vol. 31, No. 1, 1998, pp. 23-31.
- (6) S. Fricke, E. Keim and J. Schmidt, Numerical weld modeling - a method for calculating weld- induced residual stresses, *Nuclear Engineering and Design*, Vol. 206, No. 2-3, 2001, pp. 139-150.
- (7) Gary L. Cloud, Opical methods of engineering analysis, *Cambridge University Press*, 1995, pp. 453-491.
- (8) K. Creath, Phase shifting speckle interferometry, *Applied Optics*, Vol. 24, 1985, pp. 3053-3058.
- (9) S. P. Timoshenko, J. N. Goodier, Theory of elasticity (3rd-ed), *McGraw-Hill International Editions*, 1970, pp. 433-484.
- (10) T. Fuchiyama and N. Noda, Analysis of thermal stress in a plate of fuctionally gradient material, *JSAE Review*, Vol.16, 1995, pp. 263-268.